IEEE Access
Multidisciplinary | Rapid Review | Open Access Journal

Received 16 July 2023, accepted 1 August 2023, date of publication 7 August 2023, date of current version 24 August 2023.

Digital Object Identifier 10.1109/ACCESS.2023.3302924

RESEARCH ARTICLE

Lifetime Extension Technique for Voltage Source Inverters Using Selected Switching States-Based MPC Method

MINH HOANG NGUYEN[1], SANGSHIN KWAK[1], (Member, IEEE), AND SEUNGDEOG CHOI[2], (Senior Member, IEEE)

[1]School of Electrical and Electronics Engineering, Chung-Ang University, Seoul 06974, South Korea
[2]Department of Electrical and Computer Engineering, Mississippi State University, Starkville, MS 39762, USA

Corresponding authors: Sangshin Kwak (sskwak@cau.ac.kr) and Seungdeog Choi (seungdeog@ece.msstate.edu)

This work was supported in part by the National Research Foundation of Korea (NRF) Grant through the Korea Government, Ministry of Science and ICT (MSIT), under Grant 2020R1A2C1013413; and in part by the Technology Development Program to Solve Climate Changes through the NRF funded by the MSIT under Grant 2021M1A2A2060313.

ABSTRACT In a power electronic system, a control objective is to improve efficiency and reduce thermal stress in converters in order to increase the lifetime of devices. To achieve this, minimizing losses is crucial. The objective of this research paper is to present a method aimed at decreasing individually switching losses in voltage source inverters (VSI). The proposed technique uses per-phase model predictive control (MPC) with preselected switching states to target specific phase legs and achieves corresponding loss reduction. With the information of predicted reference voltages, the developed preselection algorithm determines the non-switching area of the most aged leg and corresponding switching states among available voltage vectors of VSI. The switching loss reduction in the most aged leg is achieved by selecting the optimal switching state among preselected voltage vectors based on a pre-established optimal criterion. The thermal stress of the most aged leg will be reduced, and therefore its lifetime will be increased, resulting in improving the reliability and lifetime of the entire VSI. Finally, the effectiveness of the proposed per-phase MPC method with preselection of switching state is verified by both simulation and experimental results.

INDEX TERMS Lifetime, model predictive control, per-phase, thermal reduction, preselection switching state.

I. INTRODUCTION

The two-level three-phase VSI is a popular type of power converter used in various applications such as uninterruptible power supply, wind turbine systems, and electric drive systems [1], [2]. While this converter topology is well-known, reliable, and easy to control, it is also subject to various stresses that can cause component failure and reduce its overall lifetime. As a result, increasing the lifetime of VSIs is a critical consideration in the design and operation of these systems. The components most vulnerable to failure are the dc-link capacitor and power semiconductors, with thermal stress being a major cause of failure in power modules [3], [4], [5]. The power loss in a VSI generates heat, which must be dissipated to prevent thermal stress on the components. Failure causes are mostly related to thermal stress [6], [7]. During high power loading, the semiconductor devices conduct and switch at high currents, resulting in significant power loss and heat accumulation at the chip junction. This repetitive temperature rises, and fall causes mechanical changes in materials inside the power module, leading to cracks and voids that can cause separation and failure. The temperature of the switching devices can also increase due to conduction losses, leakage current losses, and switching losses, which can be varied by modifying the switching frequency or using advanced control algorithms.

To increase the lifetime of VSIs, several techniques can be employed. One approach is to carefully select appropriate

The associate editor coordinating the review of this manuscript and approving it for publication was Sze Sing Lee.

components for the VSI circuitry. High-quality components, such as capacitors, resistors, and semiconductor devices, can improve the reliability of the system. Choosing components that are rated for higher voltage and current can also increase the overall robustness of the system. However, using higher-quality components can increase the cost of the VSI. Another technique to minimize switching losses and reduce thermal stress is to use soft-switching techniques [8], [9], [10]. Soft-switching techniques can reduce the voltage and current stress on the semiconductor devices during turn-on and turn-off. By reducing the stress on these components, their lifetime can be extended. However, implementing soft-switching techniques requires additional hardware and control, which can increase the complexity of the system and lower its reliability. Advanced gate drivers are another technique that can be used to reduce switching losses and minimize thermal stress [11], [12]. Advanced gate drivers can control the switching speed and timing of the semiconductor devices, which can reduce the stress on these components. However, similar to soft-switching techniques, using advanced gate drivers requires additional hardware and control, which can lower the system's reliability. Modulation and switching frequency variation techniques are another strategy to minimize switching losses and reduce thermal stress [13], [14], [15], [16]. Modulation techniques can vary the number of commutations in the fundamental period of the output current while switching frequency variation techniques can modify the switching time interval. Both techniques can reduce switching losses without adding extra hardware or complexity to the system.

In recent years, MPC has become increasingly popular in power electronics control due to the advancements in microprocessors [17], [18]. This nonlinear control technique optimizes the switching sequence of the VSI to minimize switching losses, leading to improved overall performance and reliability of the system. Many recent studies have shown promising results for reducing switching losses in VSI using the MPC technique. The authors of [19] propose a solution for reducing power loss using MPC by incorporating a linear low-pass filter into the objective function. This filter helps to limit thermal stress by filtering out switching states that are projected to have higher power loss. However, the accuracy of the linear filter may be affected by nonlinear constraints. The problem formulation of MPC plays a significant role in how the filter functions and nonlinear constraints could potentially mislead the filter. The author in [20] developed a switching strategy based on a predictive control technique to obtain a reduction of switching loss and balance loss in both three-phase legs. MPC offers notable flexibility in controlling multiple objectives. The conventional MPC method can incorporates an extra term in cost function, alongside control objectives such as output currents, voltage, and others, to minimize the number of switching commutations [21]. However, tuning the weighting factor for each term of the cost function can be challenging, and adding an additional cost function may decrease the output performance of the converter.

In the three-phase VSIs, unequal stress during operation or switch failure or prior replacement of switch can cause various aging conditions and expected lifetime for each phase leg. Moreover, power semiconductor devices are capable of failure due to manufacturing techniques, as they have been recognized as a possible cause. To enhance the lifetime of the entire converter, however, the active thermal control techniques in previous studies do not consider the possibility of the converter's phase legs being exposed to different aging conditions. Practically, if a phase leg has a shorter remaining useful lifetime than other phase legs, the lifetime of the entire three-phase VSI will be defined following the lifetime of the most aged phase leg. Therefore, the most aged phase leg's thermal stress should be reduced, and therefore its lifetime will be increased with the target to improve the reliability of the entire three-phase VSI. Recently, the author in [22] proposed a per-phase switching frequency MPC method by adding an additional term corresponding to phase switching frequency control to reduce switching loss of the most aged phase. However, as indicated earlier, the additional term in cost function requires an appropriate weighting factor and increases the complexity of the control scheme, whereas the increased weighting factor of switching frequency control term might deteriorate the output performance. Another attempt in [23] uses a hybrid offset voltage technique to independently adjust the switching frequency of the three-phase legs according to aging conditions. However, this technique cannot achieve minimum switching loss due to the limited clamping angle at 120°.

In this article, a per-phase MPC method with preselection of switching state is proposed to particularly relieve the loss of a specific phase leg in three-phase VSI. Based on the predicted reference voltages of three phase legs, the proposed preselection of switching state strategy instantaneously determines the non-switching area of the most aged leg and corresponding switching states among available voltage vectors of VSI. The switching loss reduction in the most aged leg is achieved by selecting the optimal switching state among preselected voltage vectors based on a pre-established optimal criterion. The thermal stress of the most aged leg will be reduced, and therefore its lifetime will be increased, resulting in improving the reliability of the entire VSI. Additionally, the output performance of VSI is guaranteed with no degradation from the proposed per-phase MPC method, and the proposed technique does not need the usage of any extra sensors or hardware modifications, which makes it easy to implement in existing systems. The proposed per-phase MPC with preselection of switching state is verified through the presentation of simulation and experiment results in three-phase VSI.

The structure of this article is divided into several sections. In Section II, the traditional MPC method for the two-level three-phase VSI is explained. Section III outlines the novel per-phase MPC approach, which includes

preselection of the switching state for minimizing switching losses. In Section IV, the results of simulations and experiments are presented, and a comparison of the output performance is made. Finally, the article concludes in Section V.

II. CONVENTIONAL MODEL PREDICTIVE CONTROL METHODS FOR VSIs

Fig. 1 illustrates the standard diagram of a two-level three-phase VSI circuit. The VSI system consists of a dc power source, a two-level three-phase VSI, and an $R-L$ load. The output current of each phase is denoted as $i_{ox}(x = a, b, c)$ while the voltage of the converter is represented by $v_x(x = a, b, c)$. The upper and lower switching states of each converter leg are referred to as S_{x1} and $S_{x2}(x = a, b, c)$, respectively.

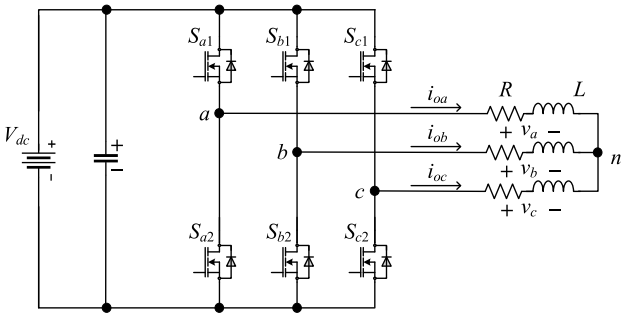

FIGURE 1. Two-level three-phase VSI with RL load circuit diagram.

By using Kirchhoff's law on the VSI circuit, we can derive equations from describing the dynamics of the load current.

$$v_x = Ri_{ox} + L\frac{di_{ox}}{dt}\ (x = a, b, c) \tag{1}$$

Predictive current control relies on a predictive model as a fundamental component, which predicts future system outputs based on past information. In order to implement the predictive control technique, the forward Euler algorithm is used on equation (1), resulting in a discrete-time expression as follows.

$$i_{ox}(k+1) = \left(1 - \frac{RT_{sp}}{L}\right) i_{ox}(k) + \frac{T_{sp}}{L} v_x(k)\ (x = a, b, c) \tag{2}$$

where T_{sp} is the sampling time. Equation (2) says the current at time instant $k+1$, $i_x(k+1)\ (x = a, b, c)$, is determined by the converter voltage and current at time instant k, denoted by $v_x(k)$ and $i_x(k)\ (x = a, b, c)$, respectively. It is a known fact that the converter voltage $v_x(k)$ can take on any of the eight possible voltage vectors shown in Fig. 2 due to the converter generating a total of eight switching states. Therefore, the current at time $k+1$, $i_x(k+1)\ (x = a, b, c)$, can be predicted to take on any of the eight current vectors calculated using equation (2). To assess the accuracy of these predictions, a cost function is required and defined as follows:

$$g_i = \left|i_x^*(k+1) - i_x(k+1)\right|\ (x = a, b, c) \tag{3}$$

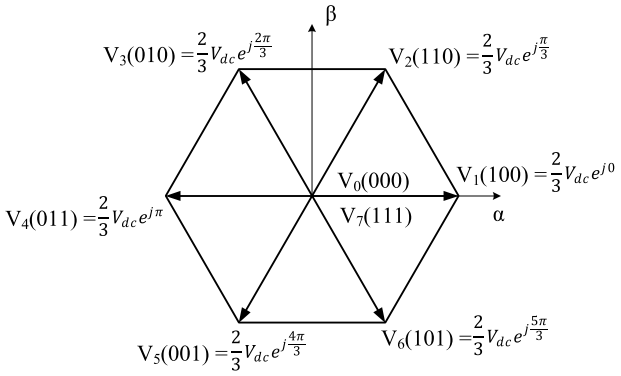

FIGURE 2. Voltage vectors of two-level three-phase VSI.

where $i_x^*(k+1)$ is the reference current for time instant $k+1$. To implement MPC, the aim is to identify the switching state that results in the lowest cost function, as defined in equation (3), and then apply it to the converter.

In conventional MPC, the approach is to choose a voltage vector that will result in the predicted current $i_x(k+1)$ being as close as possible to its reference value $i_x^*(k+1)$. Based on the predicted current values in equation (2), the optimal voltage vector $v_x^*(k)$ can be determined using the following method: substituting $i_x^*(k+1)$ for $i_x(k+1)$ in equation (2) and rearranging the equation as follows

$$v_x^*(k) = \frac{1}{T_{sp}}\left\{Li_{ox}^*(k+1) + \left(RT_{sp} - L\right) i_{ox}(k)\right\} \tag{4}$$

Equation (4) states that the current $i_x(k+1)$ will be equal to its reference value $i_x^*(k+1)$ if the converter voltage at time instant k can be set to v_x^*. Fig. 2 lists the valid voltage vectors and their corresponding switching states. Therefore, in order to implement current predictive control, the task is to select one voltage vector from the eight possibilities that meet the requirements set by the given cost function below:

$$g_v = \left|v_x^*(k) - v_x(k)\right| \tag{5}$$

This involves identifying the switching state that should be used for the power converter at time instant k by selecting the voltage vector that is closest to the "required voltage vector" $v_x^*(k)$. Fig. 3 provides a control diagram for voltage-based MPC.

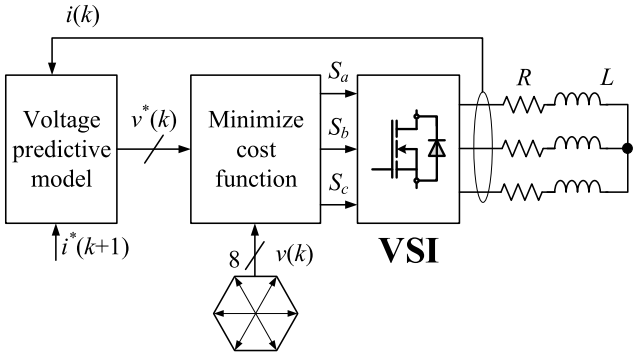

FIGURE 3. Control diagram of MPC using predicted reference voltage.

III. PROPOSED PER-PHASE MPC WITH PRESELECTION OF SWITCHING STATE

According to the analysis mentioned earlier, the phase legs of the power converter may have varying degrees of wear and tear due to factors such as manufacturing processes, uneven thermal stress distribution, and earlier replacements. This results in differences in the remaining useful lifetime among the different phase legs. Since the converter will cease to operate if one of the phase legs fails, prolonging the lifetime of the most aged leg is crucial.

In this study, the voltage-based MPC, named per-phase MPC with preselection of switching state, is used to select the best voltage vectors for a switching strategy that aims to minimize switching losses of the most aged leg. This strategy involves clamping the most aged leg of the VSI to either the positive or negative dc-link to make non-switching area. The per-phase MPC with preselection of switching state, proposed in this study, directly generates a reference voltage vector for each sampling period, which unlike the conventional MPC that only obtains load current vectors, allows for the optimization of switching patterns to minimize switching losses in the most aged leg. First, the three-phase predicted reference voltages achieved by the inverse dynamic model in (4), i.e., $v_a^*(k)$, $v_b^*(k)$, and $v_c^*(k)$, are made into a normalized form by dividing them by their peak value. The peak value for the normalization is acquired by

$$V_{peak}(k) = \sqrt{\left(v_\alpha^*(k)\right)^2 + \left(v_\beta^*(k)\right)^2} \tag{6}$$

where $v_\alpha^*(k)$ and $v_\beta^*(k)$ are the α and β components of the abc voltage vector $v_x^*(k)$ $(x = a, b, c)$ achieved by the abc-to-$\alpha\beta$ transformation. Phase a leg is regarded as being the most aged leg in this study. By considering the instantaneous magnitude of the relevant phase leg, the possible non-switching area and switching area can be chosen. The three predicted reference voltages acquired by (4) after normalization are arranged based on their magnitudes and are designated as

$$\begin{cases} v_{max}^*(k) = \max[v_{na}^*(k), v_{nb}^*(k), v_{nc}^*(k)] \\ v_{mid}^*(k) = \text{mid}[v_{na}^*(k), v_{nb}^*(k), v_{nc}^*(k)] \\ v_{min}^*(k) = \min[v_{na}^*(k), v_{nb}^*(k), v_{nc}^*(k)] \end{cases} \tag{7}$$

Assuming that phase a is the most aged leg. It can be determined that the available non-switching area corresponds to the interval that $v_{na}^*(k)$ is $v_{max}^*(k)$ or $v_{min}^*(k)$, where the switching state does not change during that interval. Meanwhile, the remaining phase legs should not be clamped to ensure that VSI operates within the linear modulation range at the available switching area, which equals the medium voltage $v_{mid}^*(k)$. This occurs because when a prohibited phase is clamped, it results in the overmodulation of at least one other phase, thereby causing a loss in the current controllability of the VSI [24]. Because three-phase voltages have 120° phase difference between them and the sum of the voltages at any time is zero. The available non-switching area of the most aged leg can be reached to 120° in both positive and negative clamping areas, as shown in Table 1. It means that the upper switch or lower switch of the most aged leg will not change its state during 120° period of time. This results in a reduction of switching frequency and corresponding switching loss.

TABLE 1. Available non-switching angle corresponding to phase *a*.

	$\theta_{n_{sw}}$	θ_{sw}
$v_{max}^*(k) = v_{na}^*(k)$	120°	x
$v_{mid}^*(k) = v_{na}^*(k)$	x	120°
$v_{min}^*(k) = v_{na}^*(k)$	120°	x

After determining the available switching area of the most aged leg, based on the sign of the corresponding reference voltage, either the upper or lower switching in the most aged phase leg is turned on. Clamping one phase between two non-prohibitive phases forms a subset among the eight voltage vectors of the VSI, with one subset consisting of four viable voltage vectors. Assuming phase a is the most aged leg, Fig. 4 illustrates the four available voltage vectors with one switch of the VSI being clamped. By selecting the optimal switching states among four preselected voltage vectors at non-switching area, the state of desired switch in the most aged leg will not change. It can be seen in Fig. 4(a); for example, the optimal switching state will be selected among four preselected voltage vectors $V_1(100)$, $V_2(110)$, $V_6(101)$,

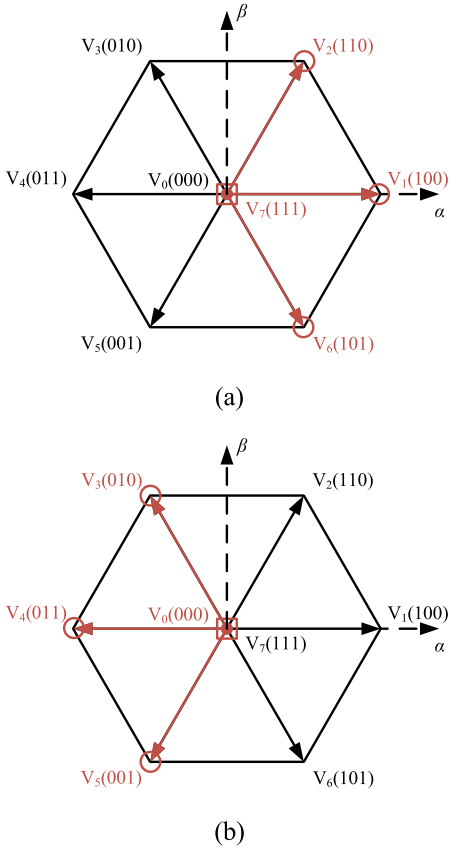

FIGURE 4. Four possible voltage vectors corresponding to upper and lower switches in phase a (a) Clamp upper switch, (b) Clamp lower switch.

and $V_7(111)$. This selection will keep turning ON the upper switch of phase *a*, which leads to an unchanged switching state and reduction of switching number. Hence, the optimal criterion defined by the cost function in (5) is employed to select one out of the four preselected voltage vectors. Table 2 shows all the preselected voltage vectors to make clamping area for particular phase leg.

TABLE 2. Preselected voltage vectors for clamping switch in different phase legs.

Phase	Clamping switch	Preselected vectors
a-phase	Upper switch	$V_1(100)$, $V_2(110)$, $V_6(101)$, and $V_7(111)$
	Lower switch	$V_0(000)$, $V_3(010)$, $V_4(011)$, and $V_5(001)$
b-phase	Upper switch	$V_2(110)$, $V_3(010)$, $V_4(011)$, and $V_7(111)$
	Lower switch	$V_0(000)$, $V_1(100)$, $V_5(001)$, and $V_6(101)$
c-phase	Upper switch	$V_4(011)$, $V_5(001)$, $V_6(101)$, and $V_7(111)$
	Lower switch	$V_0(000)$, $V_1(100)$, $V_2(110)$, and $V_3(010)$

Fig. 5 illustrates the flowchart determining the clamping area and corresponding preselection of the switching state in the proposed per-phase MPC method. When the predicted reference voltage of the most aged leg is determined as $v^*_{max}(k)$ or $v^*_{min}(k)$, the corresponding upper switch or lower switch will be clamped by using the preselection of switching state in Fig. 4 and Table 2. Thanks to this clamping area, the upper switch or lower switch will be kept turned on, resulting in the reduction of switching loss in the most aged leg. Meanwhile, when the predicted reference voltage of the most aged leg is determined as $v^*_{mid}(k)$, the eight available switching states, as in conventional MPC, are used to implement the control strategy. The maximum available clamping angle for upper or lower switch is 120°. This can be achieved by using the predefined condition in Fig. 5. Following the flowchart

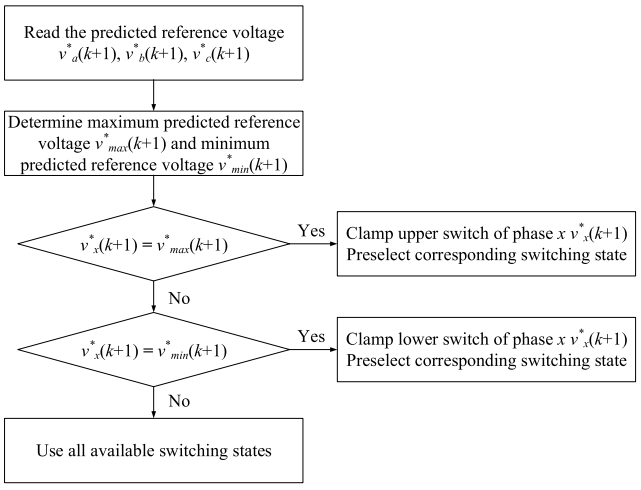

FIGURE 5. Flowchart of determining clamping area and corresponding preselection of switching state in proposed per-phase MPC method with maximum clamping angle.

in Fig. 5, the generated clamping angle will be 120° for the upper and lower switches. The total clamping angle in one phase leg can be achieved up to 240° by using the proposed per-phase MPC method. Fig. 6 shows the switching pattern acquired by proposed per-phase MPC with preselection of switching state with maximum clamping angle when phase *a* is assumed as the most aged phase leg. As can be seen in Fig. 6, when the predicted reference voltage of phase *a* is determined as $v^*_{max}(k)$ or $v^*_{min}(k)$, the corresponding upper switch or lower switch of phase *a* will be clamped by using the preselected switching states.

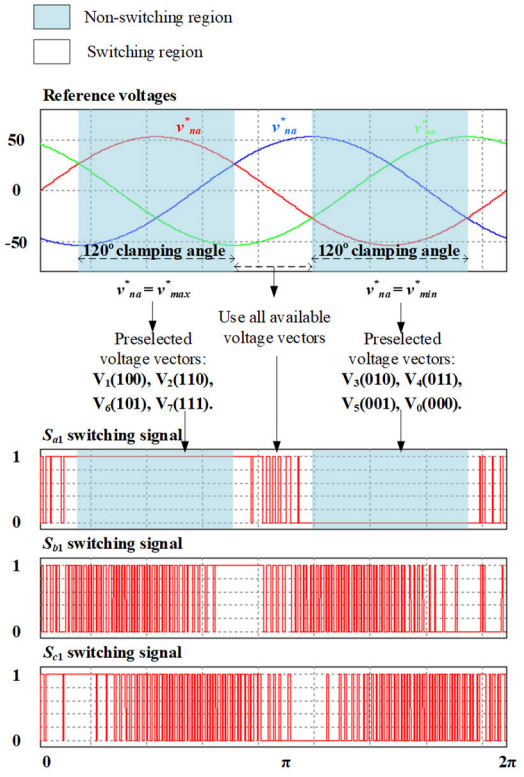

FIGURE 6. Switching pattern acquired by proposed per-phase MPC with preselection of switching state with maximum clamping angle.

The width of clamping area can be varied by adjusting the clamping angle $\theta_{n_{sw}}$. To change the value of clamping angle of upper clamping area, an upper limit L_{up} will be added to predefined condition, whereas a lower limit L_{low} will be added to predefined condition to define lower clamping area. The upper and lower limits can be expressed as follows

$$L_{up} = V_{peak} \times \cos\left(\theta_{n_{sw}}/2\right) \tag{8}$$

$$L_{low} = -V_{peak} \times \cos\left(\theta_{n_{sw}}/2\right) \tag{9}$$

The clamping angle $\theta_{n_{sw}}$ ranges from 0° to 120°. Fig. 7 illustrates the flowchart determining the clamping area and corresponding preselection of the switching state in the proposed per-phase MPC method with adjustable clamping angle.

To account for the delay that naturally occurs within the controller, the inverse model in equation (4) is adjusted by

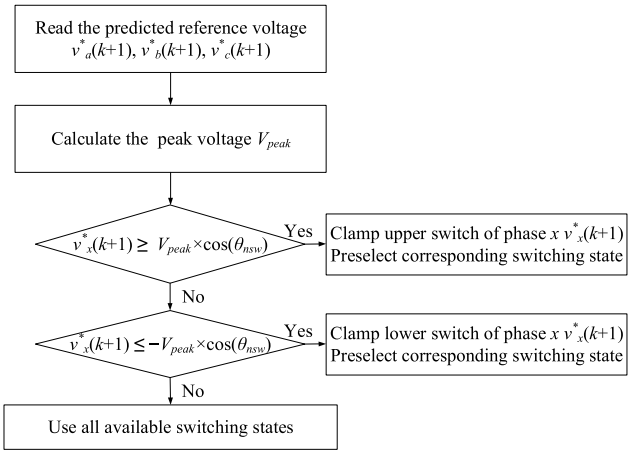

FIGURE 7. Flowchart of determining clamping area and corresponding preselection of switching state in proposed per-phase MPC method with adjustable clamping angle.

advancing it by one step. As a result, the predicted reference voltage at the $(k+1)$ th moment can be derived.

$$v_x^*(k+1) = \frac{1}{T_{sp}}\left\{Li_x^*(k+2) + \left(RT_{sp} - L\right) i_x(k+1)\right\} \tag{10}$$

To obtain the one-step predicted output current $i_x(k+1)$ $(x = a, b, c)$ needed for (7), the measured output current $i_x(k)$ and the present VSI voltage application $v_x(k)$, as shown in (4), are used. Additionally, the Lagrange extrapolation technique can be employed to determine the predicted reference currents, $i_x^*(k+1)$ and $i_x^*(k+2)$ $(x = a, b, c)$, based on the present and the two past reference values. This can be described as follows:

$$i_x^*(k+1) = 3i_x^*(k) - 3i_x^*(k-1) + i_x^*(k-2) \tag{11}$$

$$i_x^*(k+2) = 3i_x^*(k+1) - 3i_x^*(k) + i_x^*(k-1) \tag{12}$$

Finally, the following cost function, which evaluates the modified predicted reference voltage with the predicted zero-sequence voltage injection, is described as follows

$$g_v = \left|v_x^{**}(k+1) - v_x(k+1)\right| \; (x = a, b, c) \tag{13}$$

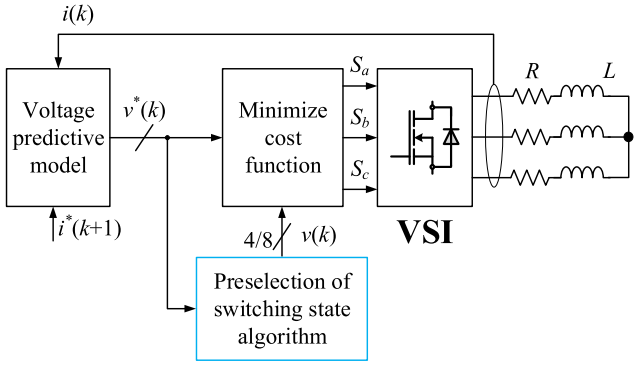

FIGURE 8. Block diagram of the proposed per-phase MPC method with preselection of switching state.

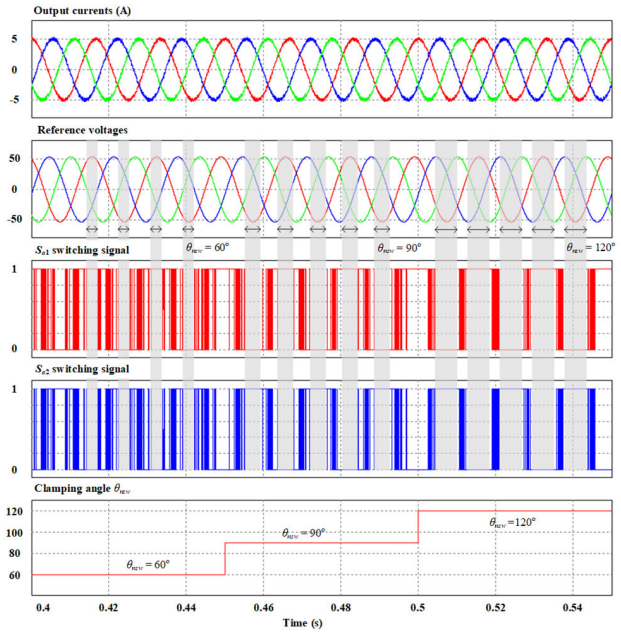

FIGURE 9. Simulation results of output currents and switching patterns waveforms acquired by proposed per-phase MPC with different clamping angle.

By comparing the block diagram in Fig. 8 with the conventional method shown in Fig. 3, it becomes evident that the proposed per-phase MPC technique with preselection of switching state can be implemented without requiring any additional components. Furthermore, additional information regarding the load power factor is unnecessary as the algorithm relies on sampled values of the reference voltage to identify the suitable switch to control during each sampling period. By employing the proposed per-phase MPC with preselection of switching state, the most aged phase leg in VSI can be operated with minimum switching loss, regardless of the operating conditions being steady-state or transient.

IV. VERIFICATION RESULTS

A. SIMULATION AND EXPERIMENT RESULTS

To validate the proposed per-phase MPC with preselection of switching state approach, the PSIM simulation tool is used to implement the two-level three-phase VSI depicted in Fig. 1. The specifications for the two-level three-phase VSI can be found in Table 3.

TABLE 3. Parameter of two-level three-phase VSI system.

Parameters	Value
DC-link voltage V_{dc} (V)	200
DC-link capacitance (μF)	680
Load resistance R (Ω)	10
Load inductance L_f (mH)	10
Load angle (degree)	20
Sampling frequency (kHz)	20
Fundamental frequency (Hz)	60
Reference current (A)	5

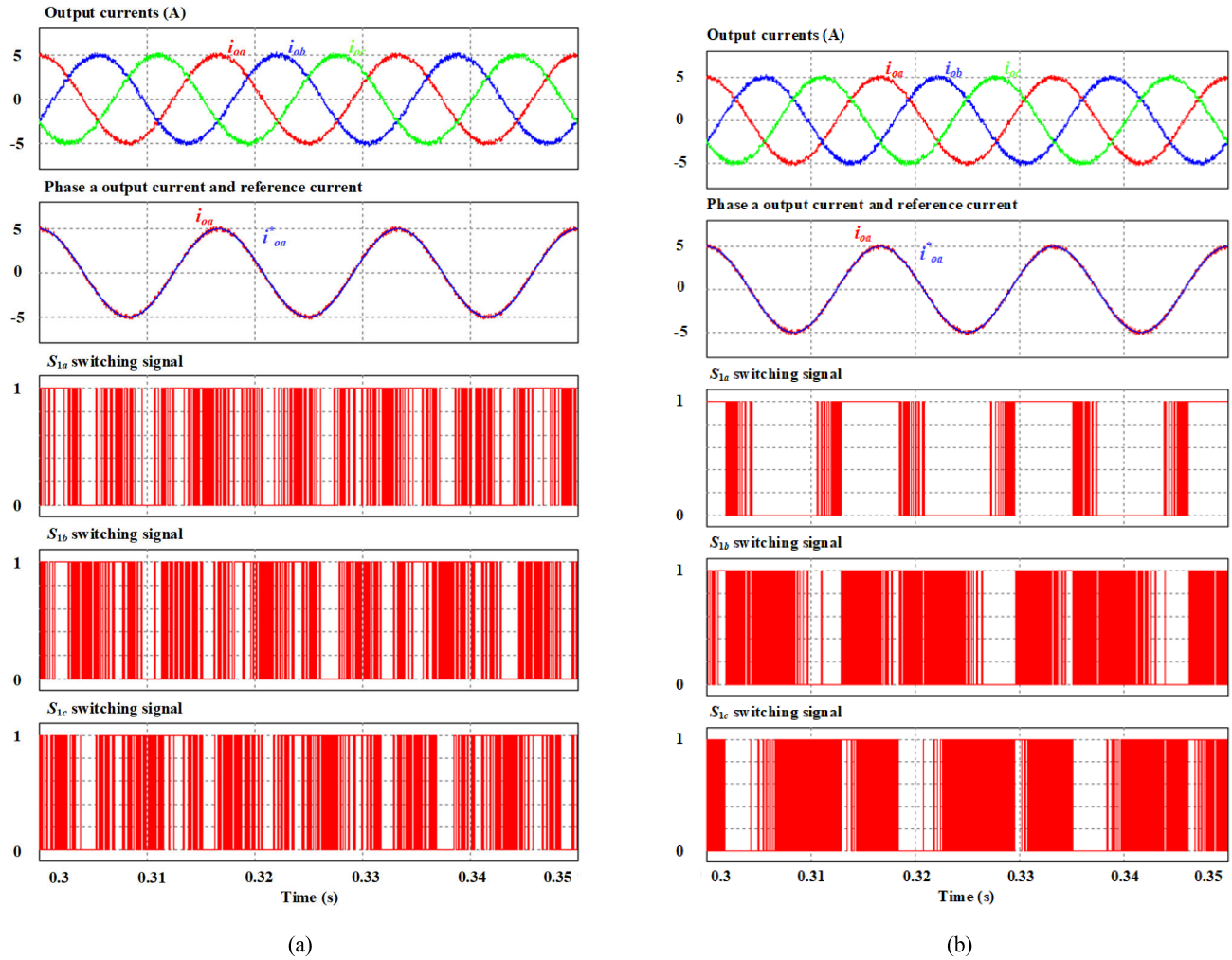

FIGURE 10. Simulation results of output currents and switching patterns waveforms at steady-state acquired by (a) conventional MPC, (b) proposed per-phase MPC.

In this simulation section, phase *a* is assumed to be the most aged leg. The proposed per-phase MPC will be applied to reduce the switching frequency of phase *a*, which lowers the corresponding switching loss and increase lifetime of VSI. Fig. 9 shows the phase output currents, reference voltages, and phase *a* switching patterns waveforms with the change of clamping angle acquired by the proposed per-phase MPC method. The clamping angle is set at three different values including 60°, 90°, and 120°. It can be observed that the proposed per-phase MPC technique generates sinusoidal currents, which are accurate with regard to phase and magnitude. The clamping areas following are generated precisely following the change clamping angles, where the change of width of clamping areas is noticeable. This result verifies the correct operation of the proposed per-phase MPC method at different clamping angles.

Fig. 10 depicts the waveforms of the output currents and corresponding switching patterns acquired by the conventional MPC and the proposed per-phase MPC methods at steady-state. The proposed per-phase method with the maximum clamping angle of 120° is implemented. In Fig. 10(a), the output currents acquired from conventional MPC are sinusoidal and correct in magnitude and phase. It can be seen that, for example, the phase *a* output current tracks correctly the corresponding reference current. Regarding the proposed per-phase MPC method in Fig. 10(b), phase *a* is considered the most aged leg. Therefore, the switching loss of phase *a* should be decreased to extend the lifetime of VSI. To implement the proposed per-phase MPC method, when the predicted reference voltage of the most aged leg, phase *a*, is determined as $v^*_{max}(k)$ or $v^*_{min}(k)$, the corresponding upper switch or lower switch will be clamped by using the preselection of switching state in Fig. 5. As shown in Fig. 10(b), the switching pattern of the upper switch in phase *a* contains 120° non-switching area as expected. It means that the upper switch of phase *a* does not change the state for 120° period of time. It is similar in the lower switch. Hence, the switching frequency and corresponding switching loss of phase *a* is lowered. Additionally, the output currents acquired by the proposed per-phase MPC approach are sinusoidal and correct in magnitude and phase as the conventional MPC scheme. It verifies that the proposed per-phase MPC

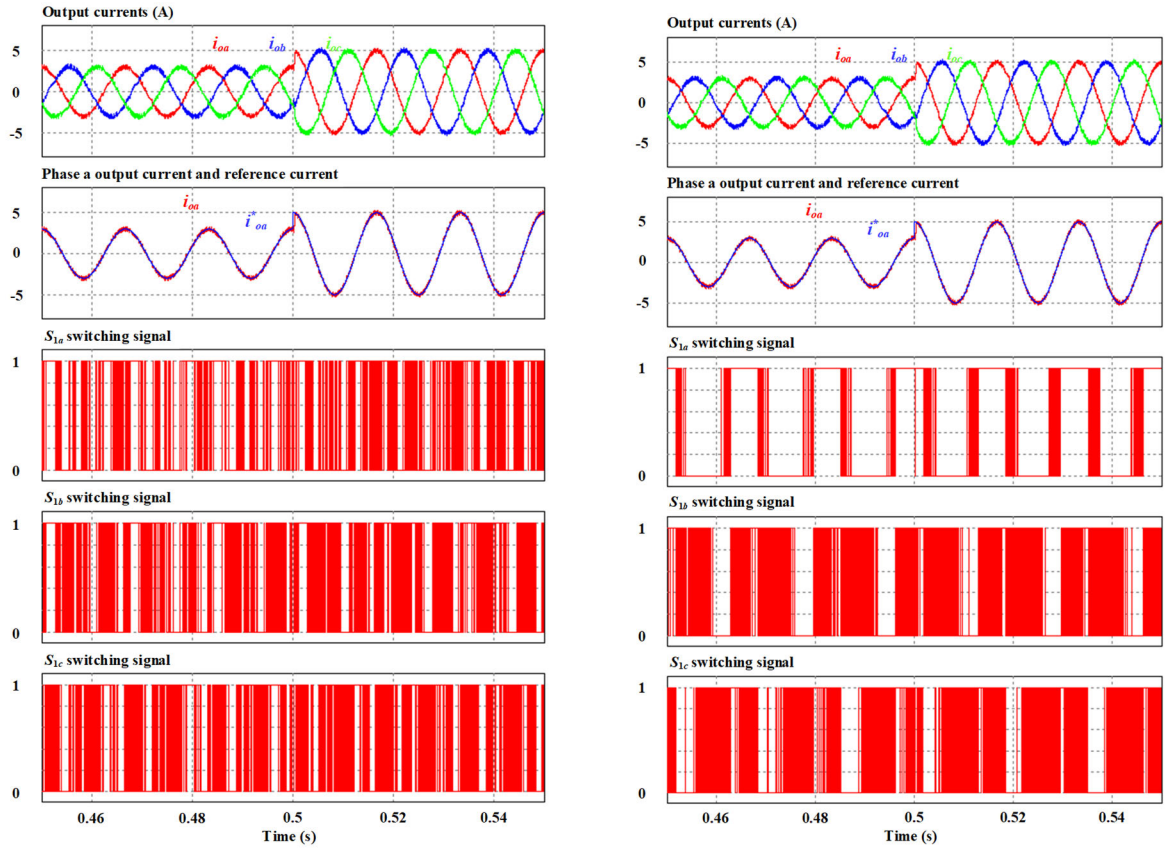

FIGURE 11. Simulation results of output currents and switching patterns waveforms at transient-state acquired by (a) conventional MPC, (b) proposed per-phase MPC.

approach works correctly and does not deteriorate the output performance.

The dynamic responses for the conventional MPC method and proposed per-phase MPC methods are shown in Fig. 11(a) and (b), respectively. The amplitude of the reference currents is changed from 3 A to 5 A at time t = 0.5s. It can be observed that the output currents of the proposed per-phase MPC method have a similar dynamic response as in the conventional MPC. The output current of phase *a* acquired by the proposed per-phase MPC method correctly follows the corresponding reference current with a fast dynamic response. Additionally, thanks to the proposed per-phase MPC method, the switching pattern of the upper switch in phase *a* contains 120° non-switching area as expected.

The conventional MPC and proposed per-phase MPC method are implemented by configuring a prototype setup. The platform of the two-level three-phase VSI (with the circuit topology shown in Fig. 1) is shown in Fig. 12, and the system parameters are similar to those in the simulation section, as shown in Table 3. The conventional MPC and proposed MPC method are executed using a TI digital signal processor (DSP) TMS320F28335 for VSI.

Fig. 13 and 14 present the experiment waveforms of output currents and corresponding switching patterns acquired at steady-state acquired by the conventional MPC and proposed

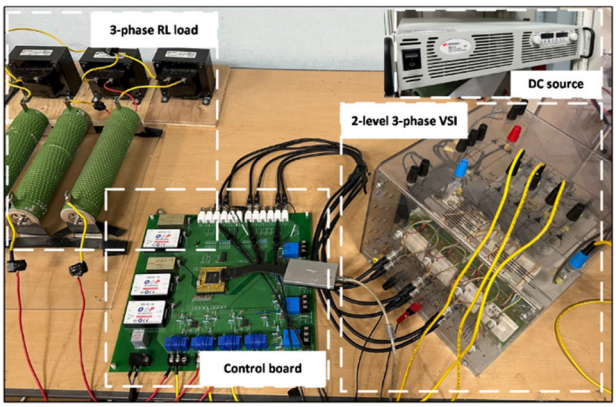

FIGURE 12. Overall experimental setup including two-level three-phase inverter, DC power source, load and control board.

per-phase MPC approaches. In Fig. 13(a), the output currents acquired from conventional MPC are sinusoidal and correct in magnitude and phase. The experimental waveforms of output current and switching patterns acquired by the conventional MPC method are similar to the simulation results. Regarding the proposed per-phase MPC method in Fig. 13(b), phase *a* is considered the most aged leg. Therefore, the switching loss of phase *a* should be decreased to extend the lifetime of VSI. To implement the proposed per-phase

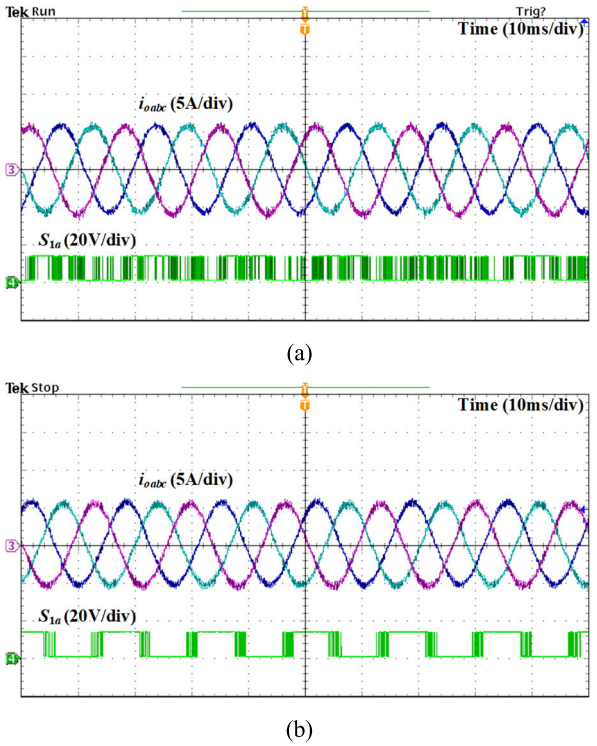

FIGURE 13. Experimental results of output currents and phase a switching patterns waveforms at steady-state acquired by (a) conventional MPC, (b) proposed per-phase MPC.

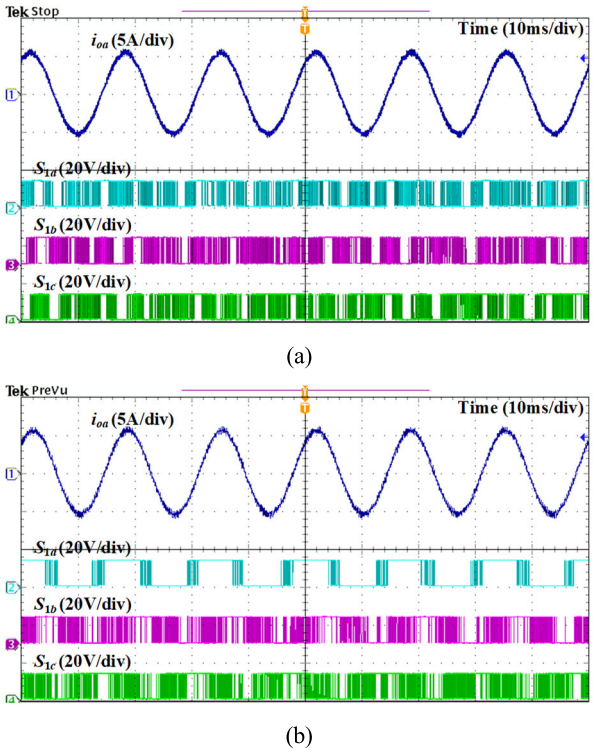

FIGURE 14. Experimental results of phase a output current and switching patterns waveforms at steady-state acquired by (a) conventional MPC, (b) proposed per-phase MPC.

MPC method, when the predicted reference voltage of the most aged leg, phase a, is determined as $v^*_{max}(k)$ or $v^*_{min}(k)$, the corresponding upper switch or lower switch will be clamped by using the preselection of switching state in Fig. 5. As shown in Fig. 13(b), the switching pattern of the upper switch in phase a contains 120° non-switching area as expected. As observed from Fig. 14(b), the experimental waveforms of three-phase switching patterns acquired by the proposed per-phase MPC method are similar to the simulation results in Fig. 10(b). Additionally, the output currents acquired by the proposed per-phase MPC method are sinusoidal and correct in magnitude and phase as the conventional MPC method and simulation results. The experimental results at steady-state verify that the proposed per-phase MPC method works correctly.

The experimental waveforms of dynamic responses for the conventional MPC method and proposed per-phase MPC methods are shown in Fig. 15(a) and (b), respectively. The amplitude of the reference currents is changed from 3 A to 5 A. It can be observed that the output currents of the proposed per-phase MPC method have a similar dynamic response as in the conventional MPC. The output current of phase a acquired by the proposed per-phase MPC method correctly follows the corresponding reference current with a fast dynamic response. Additionally, thanks to the proposed per-phase MPC method, the switching pattern of the upper switch in phase a contains 120° non-switching area as expected. The experimental results at the transient state verify that the proposed per-phase MPC method does not degrade the dynamic performance of VSI, whereas generating a non-clamping area for the most aged leg correctly (assuming phase a is the most aged leg).

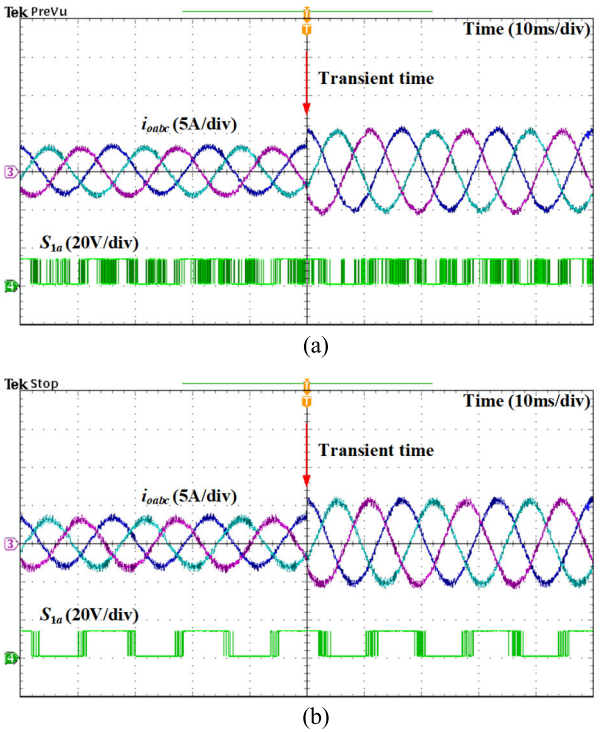

FIGURE 15. Experimental results of output currents and phase a switching patterns waveforms at transient-state acquired by (a) conventional MPC, (b) proposed per-phase MPC.

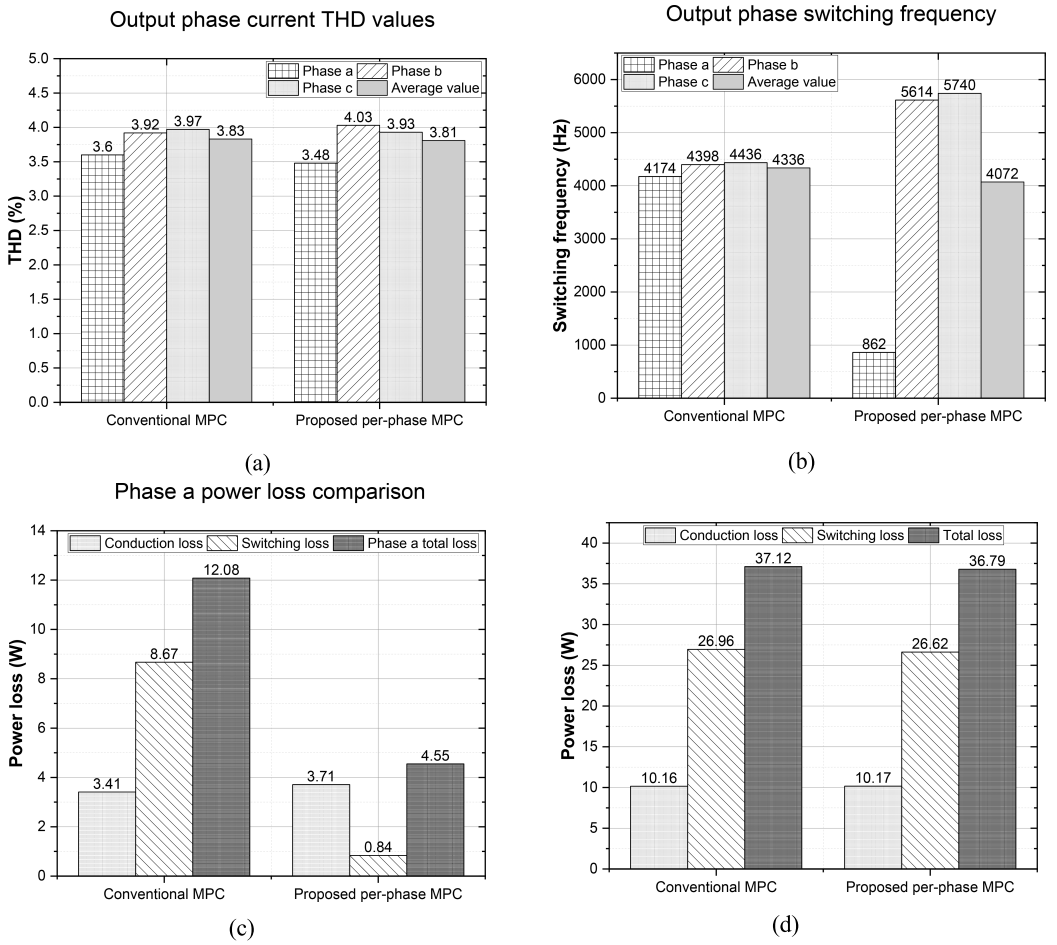

FIGURE 16. Comparison of (a) output currents THD, (b) phase switching frequency, (c) phase a power loss, and (d) total loss of VSI acquired by the conventional MPC and proposed per-phase MPC methods ($V_{dc} = 200V$, $T_{sp} = 50\mu s$, load angle $\varphi = 20°$, $I^* = 5A$).

B. PERFORMANCE COMPARISON

In order to evaluate the superiority of the proposed per-phase MPC method in terms of output performance, switching frequency reduction capability, and switching loss reduction capability, the calculated values from simulation results are presented.

Fig. 16(a) shows the comparison of output phase current total harmonic distortion (THD) values between the conventional MPC and proposed per-phase MPC methods. Phase *a* is assumed that be the most aged leg, which requires switching loss reduction. It can be seen that the phase output current THD values change slightly when applying the proposed per-phase MPC method. Meanwhile, the average values of phase output current THD acquired by the two control schemes are similar at about 3.8%. Hence, this result can confirm that the proposed per-phase MPC method does not deteriorate the output performance of VSI. Regarding the comparison of output phase switching frequency in Fig. 16(b), it can be seen that the switching frequency of phase *a* acquired by the proposed per-phase MPC method is decreased by about 80% compared to that of the conventional MPC method. Thanks to the 120° non-switching areas, generated using preselection of switching state algorithm, the switching frequency of the most aged leg can be reduced significantly. Although the switching frequencies of phases *b* and *c* acquired by the proposed per-phase MPC method increase by about 30% compared to that of the conventional MPC method, the average value of output switching frequency from the proposed per-phase method is lowered than that of conventional MPC method. In Fig. 16(c), the conduction loss and switching loss of phase *a* acquired by two control schemes are compared. It can be realized that due to the reduction of switching frequency in phase *a* acquired by the proposed per-phase MPC method, the corresponding switching loss is lowered by about 90% compared to that of the conventional MPC method. The conduction loss of phase *a* acquired by the proposed per-phase MPC method slightly increases compared to the conventional MPC method. Thus, the phase *a* power loss acquired by the proposed per-phase method is lowered by about 60% from the conventional MPC method. This helps reduce the thermal stress on phase *a* leg and extends the corresponding lifetime of both phase leg *a* and the entire VSI. Fig. 16(d) shows the conduction loss, switching loss, and total loss of VSI acquired by two

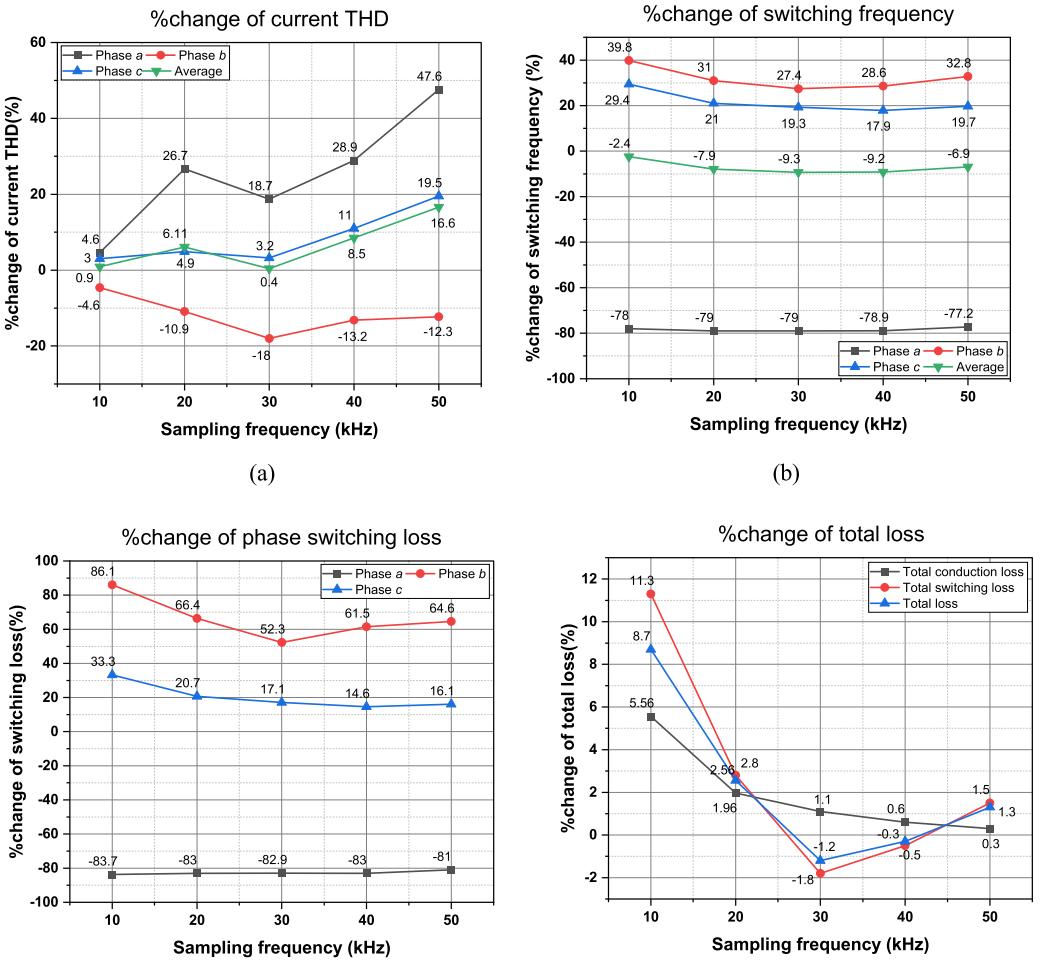

FIGURE 17. Characteristic of output performance acquired by proposed per-phase MPC with preselection of switching state method compared to conventional MPC versus the change of sampling frequency in terms of (a) Output current THD, (b) Phase switching frequency, (c) Phase switching loss, (d) Total loss (V_{dc} = 200V, load angle $\theta = 20°$ and $I^* = 5A$).

control schemes. Due to the increase of switching frequency in phase b and c in the proposed per-phase MPC method, the total switching loss of VSI acquired by the two control schemes is similar. The total loss acquired by the two control schemes is almost the same.

To provide a clearer understanding of the performance of the proposed per-phase MPC with preselection of switching state method, a comprehensive comparison is carried out where phase a is assumed to be the most aged phase leg. The percentage of variation in terms of various aspects, such as output current THD, phase switching frequency, phase switching loss, and total loss acquired by the proposed per-phase MPC technique compared to conventional MPC is described as

$$\%\text{change of } x = \frac{x_{Proposed\ per-phase\ MPC} - x_{Conventional\ MPC}}{x_{Conventional\ MPC}} \times 100\% \quad (14)$$

where x can be various aspects of current THD, switching frequency, switching loss, and total loss. Additionally, $x_{Proposed\ per-phase\ MPC}$ and $x_{Conventional\ MPC}$ represent the performance aspects yielded by proposed per-phase MPC and conventional MPC methods, respectively. The negative value of %change of x indicates the reduction of the corresponding performance aspect acquired by the proposed per-phase MPC with preselection of switching state technique compared to conventional MPC, whereas the positive value indicates the increase.

Fig. 17(a) depicts the %change of current THD acquired by the proposed per-phase MPC compared to conventional MPC methods under the change of sampling frequency. Due to the objective of minimizing switching frequency of phase a, the per-phase MPC with preselection of switching state exhibits a relatively higher THD in the output current of phase a compared to conventional MPC. Additionally, when the sampling frequency is smaller than 50 kHz, the increase of average THD acquired by the proposed per-phase MPC is insignificant. Regarding the phase switching frequency, Fig. 17(b) indicates that the proposed per-phase MPC successfully lowers the switching frequency of the most aged

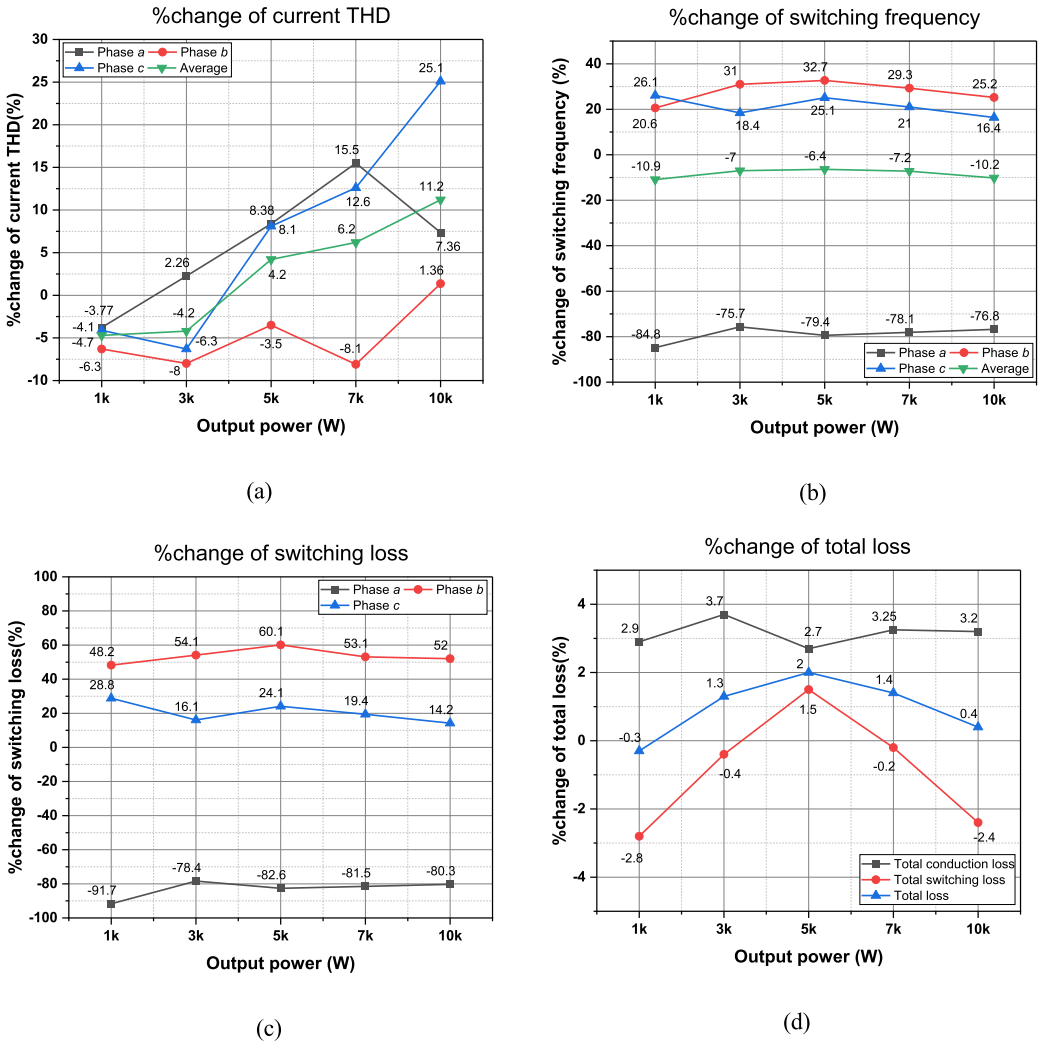

FIGURE 18. Characteristic of output performance acquired by proposed per-phase MPC with preselection of switching state method compared to conventional MPC versus the change of output power in terms of (a) Output current THD, (b) Phase switching frequency, (c) Phase switching loss, (d) Total loss (V_{dc} = 720V, load angle $\theta = 20°$ and f_{sp} = 20kHz).

phase leg *a*, where the reduction of switching frequency in phase *a* is reached about 79%. Although the switching frequency of phase *b* increases by around 30%, and that of phase *c* increases by approximately 20%, it does not exert a negative impact on the two-level three-phase VSI when the most aged leg still can be prolonged its lifetime and delay its failure until the next maintenance. Additionally, the increase of switching frequency in the two remaining phase legs will lead to the balance of aging conditions between the three phase legs. Thanks to the reduction of switching frequency in the most aged phase leg *a*, the proposed per-phase MPC method can reduce corresponding switching loss of phase *a* up to 84% compared to conventional MPC, as shown in Fig. 17(c). Due to the difference in conduction loss between the two approaches is negligible. Thus, the total conduction loss, total switching loss, and total loss of the proposed MPC with preselection of switching state are comparable to those of the conventional MPC across various sampling frequency conditions, as shown in Fig. 17(d).

Fig. 18(a) illustrates the %change of current THD acquired by the proposed per-phase MPC compared to conventional MPC methods under the change of output power. At low output power, the proposed per-phase MPC with preselection of switching state even lowers the output current THD compared to the conventional MPC. When the output power is higher than 5 kW, the per-phase MPC with preselection of switching state exhibits a slightly higher average THD compared to conventional MPC. Regarding the phase switching frequency, Fig. 18(b) indicates that the proposed per-phase MPC successfully lowers the switching frequency of the most aged phase leg *a*, where the reduction of switching frequency in phase *a* is reached about 80%. Meanwhile, the switching frequency of the remaining phase legs acquired by the proposed per-phase MPC with preselection of switching state has increments ranging from 20% to 30% compared to conventional MPC scheme. In terms of the average switching frequency, the proposed per-phase MPC with preselection of switching has a lower average switching frequency compared

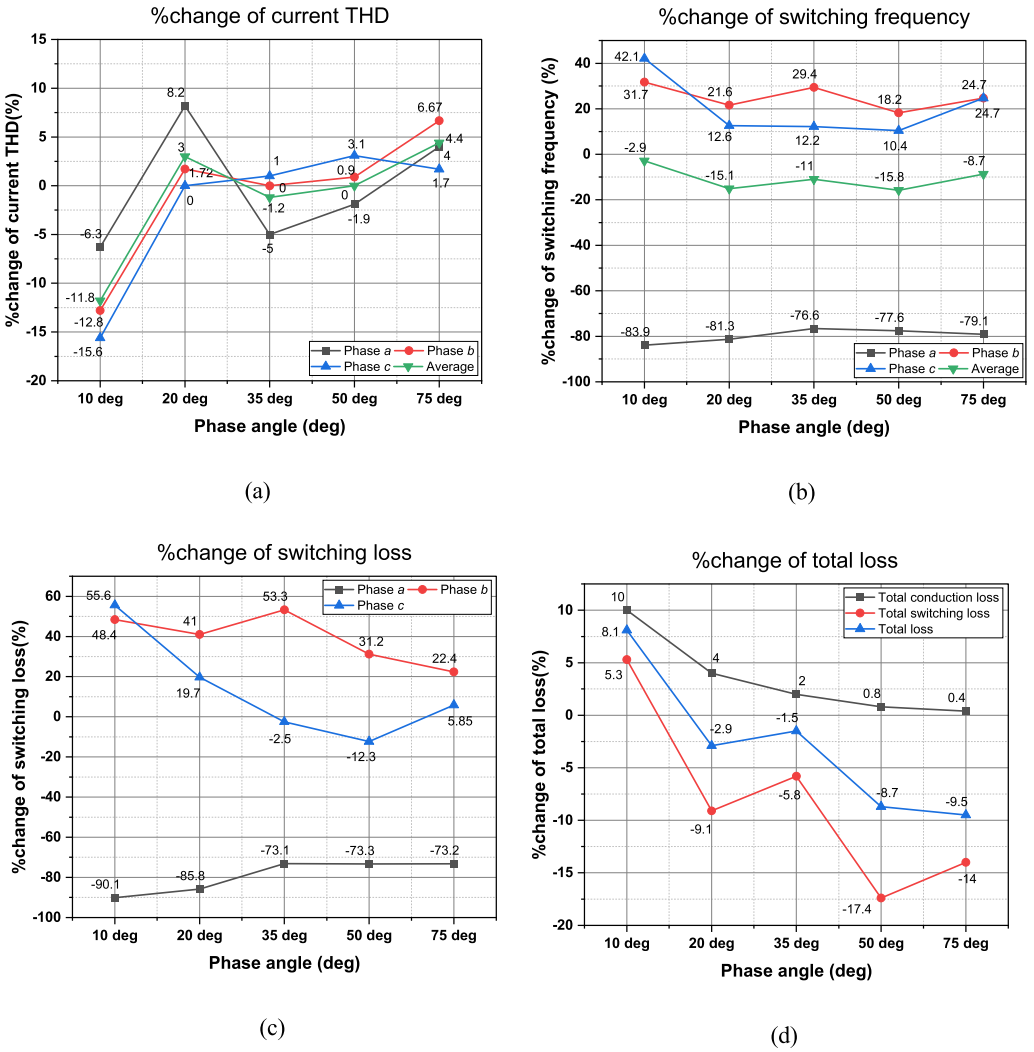

FIGURE 19. Characteristic of output performance acquired by proposed per-phase MPC with preselection of switching state method compared to conventional MPC versus the change of load condition in terms of (a) Output current THD, (b) Phase switching frequency, (c) Phase switching loss, (d) Total loss ($V_{dc} = 720V$, load angle $\theta = 20°$ and $f_{sp} = 20kHz$).

to conventional MPC under different output power conditions. Thanks to the reduction of switching frequency in the most aged phase leg *a*, the proposed per-phase MPC method can reduce corresponding switching loss of phase *a* up to 90% compared to conventional MPC at low output power and about 80% at other output power conditions, as shown in Fig. 18(c). The total conduction loss, total switching loss, and total loss of the proposed MPC with preselection of switching state are comparable to those of the conventional MPC across various output power conditions, as shown in Fig. 18(d).

In terms of load conditions change, it is generated by increasing the load inductance to modify the load phase angle. Fig. 19(a) shows the %change of output current THD acquired by the proposed per-phase MPC method under different load conditions. It can be seen that when the load phase angle is less than or equal to 50°, the proposed per-phase MPC method exhibits a similar average THD to conventional MPC where the %change of output current THD is negligible. Meanwhile, even at a greater load phase angle of 75°, the increase of output current THD acquired by the proposed MPC technique is relatively small. As for switching frequency performance, Fig. 19(b) indicates that the proposed per-phase MPC successfully lowers the switching frequency of the most aged phase leg *a*, where the reduction of switching frequency in phase *a* is reached to about 84% at a small load phase angle. The reduction in switching frequency of phase *a* decreases to roughly 80% as the load phase angle rises. In terms of average switching frequency, the proposed per-phase MPC with preselection of switching state exhibits a slightly lower average switching frequency compared to the conventional MPC across different load phase angles. When considering the %change of switching loss in Fig. 19(c), the per-phase MPC approach with preselection of switching state significantly reduces the switching loss of phase *a*. Specifically, it achieves a reduction of approximately 90% at small load phase angles compared to the conventional MPC and

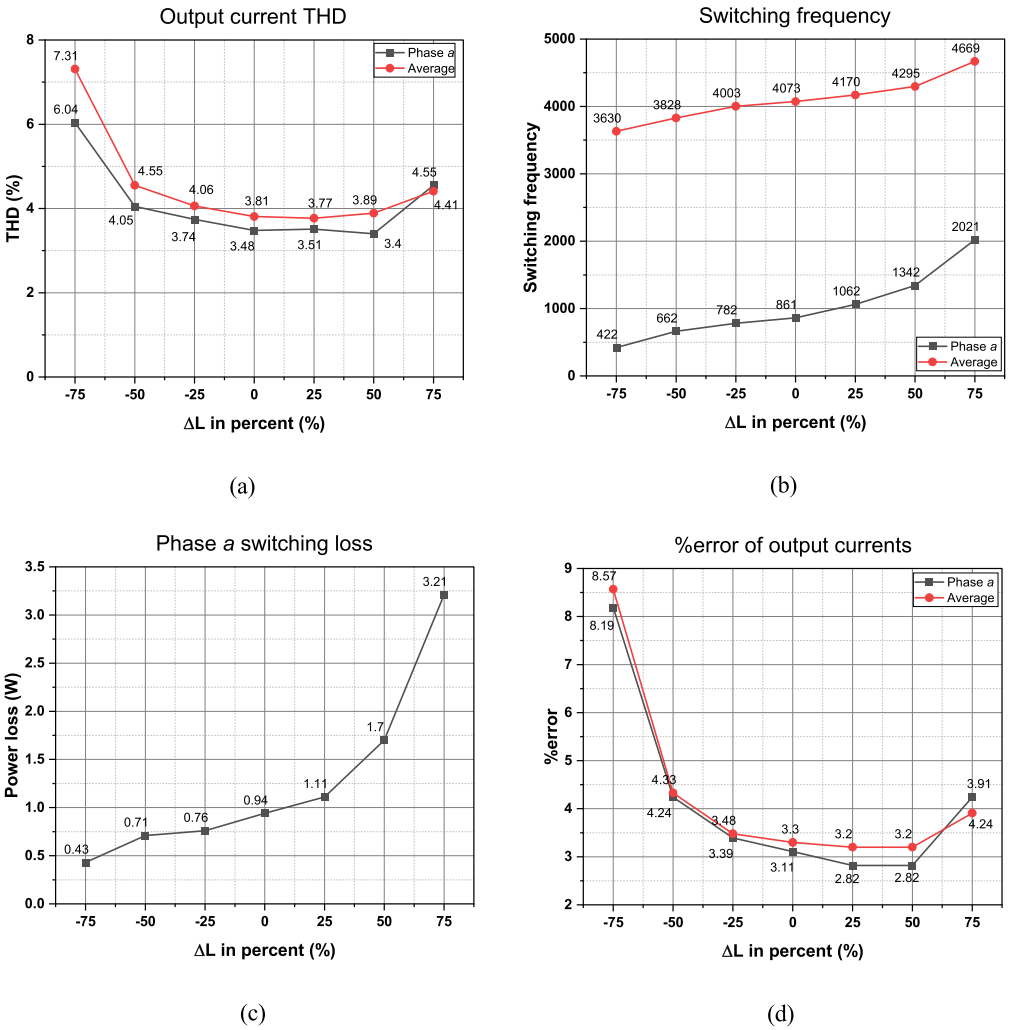

FIGURE 20. Comparison results acquired by proposed per-phase MPC with preselection of switching state methods versus parameter error in the load inductance (a) output current THD, (b) switching frequency, (c) phase a switching loss, (d) %error of load currents.

about 80% at large load phase angles. The proposed per-phase MPC with preselection of switching state method results in an increase of switching loss for phase *b* and *c* compared to the conventional MPC, ranging from 10% to 40%, depending on the load condition. As can be seen in Fig. 19(d), the total switching loss and total loss acquired by the proposed per-phase MPC with preselection of switching state are lower than that of conventional MPC when the phase angle is greater than 20°.

Fig. 20 illustrates the performance comparison of various parameters, including output current THD, switching frequency, power loss, and %error of output current with respect to model load inductance error. As can be seen in Fig. 20(a), the phase *a* and average output current THD slightly change with 50% smaller and 75% larger load inductance error. Notably, when the parameter of load inductance is 75% smaller than the actual inductance, the output current THD experiences a significant increase. Fig. 20(b) and (c) depict that the capability of switching frequency reduction of proposed MPC method is lowered when the parameter of load inductance is larger than the actual one. The %error of output current slightly changes with 50% smaller and 75% larger load inductance error. When the parameter of load inductance is 75% smaller than the real inductance, the %error of output current rise significantly, reaching approximately 2.6 times compared to normal condition.

Fig. 21 illustrates the performance comparison of various parameters, including output current THD, switching frequency, power loss, and %error of output current with respect to model load resistance error. As can be seen in Fig. 21(a), the phase *a* and average output current THD slightly change with 25% smaller and 75% larger load resistance error. When the parameter of load resistance is 75% smaller than the real resistance, the output current THD significantly increases. Fig. 21(b) shows that the capability of switching frequency reduction of proposed MPC method is well maintained under model load resistance error. The %error of output current slightly changes with 50% smaller and 75% larger load resistance error. When the parameter of load resistance is 75% smaller than the real resistance, the %error of output current

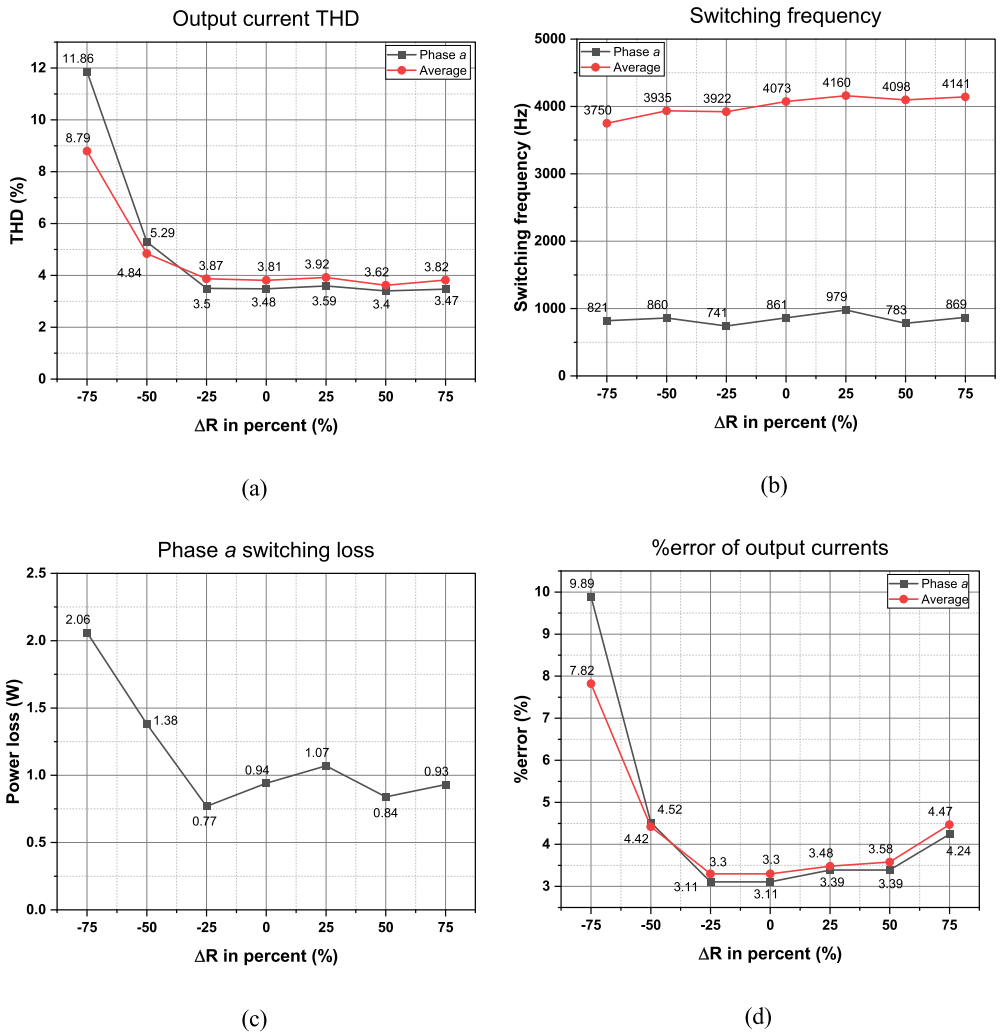

FIGURE 21. Comparison results acquired by proposed per-phase MPC with preselection of switching state methods versus parameter error in the load resistance (a) output current THD, (b) switching frequency, (c) phase a switching loss, (d) %error of load currents.

increases significantly by about 2.4 times compared to normal condition.

As it was revealed that thermal stress is the most critical failure cause of the power semiconductor devices, which decreases the lifetime of switching devices and entire converter. To investigate the effectiveness of the proposed per-phase MPC method on the lifetime of the power semiconductor devices, the flowchart for lifetime estimation shown in Fig. 22 is conducted. As shown in Fig. 22, a predefined mission profile is applied on the VSI, where the output power of converter is periodically changed between 14kW to 5.5kW. The loss on power semiconductor devices can be calculated using the thermal module in PSIM simulation program and the corresponding thermal characteristics of the device.

The thermal model (i.e., the network of thermal resistance and capacitance) can transfer the acquired power loss to the junction temperature of power semiconductor devices. In this case, a Foster-type thermal network [25] is conducted, as presented in Fig. 23. The $n-$ thermal resistance is denoted by $R_{th,n}$, whereas $n-$thermal time constant is denoted by τ_n.

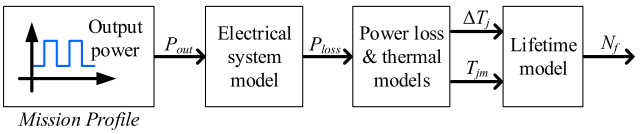

FIGURE 22. Flowchart for lifetime estimation of power semiconductor devices caused by predefined mission profile.

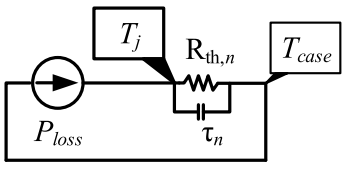

FIGURE 23. n−layers Foster-type network.

Generally, the Foster-type thermal network with $n = 3$ or 4 is usually used. T_j and T_{case} are the junction temperature and case temperature, respectively. It is assumed that T_{case}

has value of 50°C. The corresponding parameters of three layers Foster thermal network are adopted from the datasheet of switching device [26].

Fig. 24 displays the calculated junction temperature and three-phase output currents as they vary with changes in output power within the mission profile. The simulation is run using both the conventional MPC method and the proposed per-phase MPC scheme following the predefined mission profile. As depicted in Fig. 24(a), the conventional MPC method yields a temperature variation ΔT_j amplitude of 35°C. In the second simulation, the proposed per-phase MPC method is used, assuming that phase a is the most aged leg. With the same boundary conditions, the proposed per-phase MPC with preselection of switching state method lowers the temperature variation in phase a to 25°C at, as depicted in Fig. 24(b).

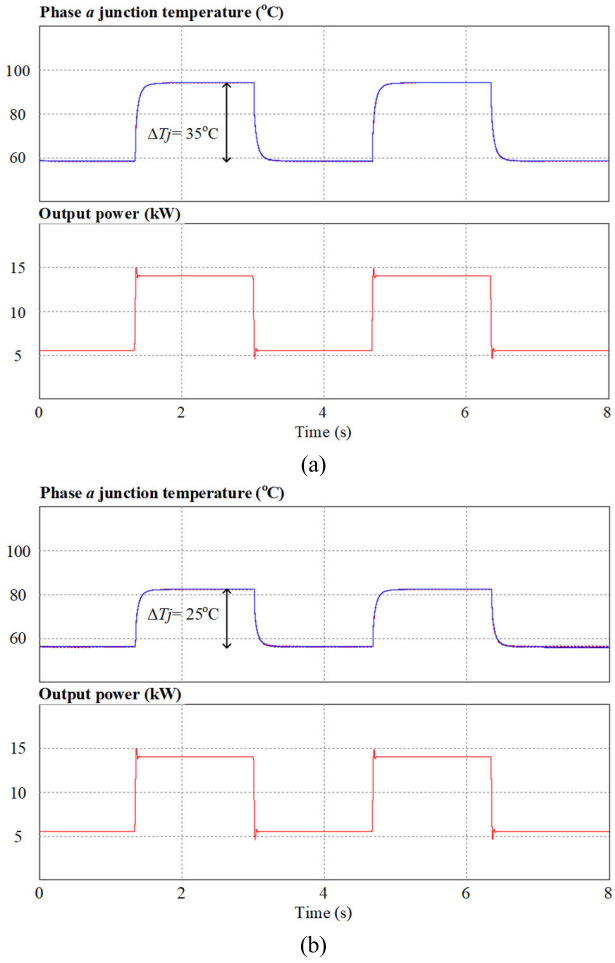

FIGURE 24. Junction temperature of transistor in phase a and output currents acquired by (a) conventional MPC, (b) proposed per-phase MPC method.

Analytical models that are commonly used to describe the correlation between the parameters of temperature cycles and the number of cycles to failure N_f will be used in order to determine the lifetime of power semiconductor devices. The Coffin-Manson model from [27] is conducted in this investigation. The Coffin-Manson model with corresponding parameters acquired by [28] and [29] is applied in this paper for a rough approximation, shown in (15)

$$N_f = 1.017^{(125-T_{jm}-\Delta T_j/2)^{1.16}} \times 8.2 \times 10^{14} \times \Delta T_j^{-5.28} \tag{15}$$

By applying Coffin-Manson model shown in (15), it can determine the number of cycles that the power semiconductor devices can endure before failing following the established mission profile. The estimated lifetime is presented in Table 4. The investigation found that implementing the proposed per-phase MPC method to decrease temperature variation results in an approximately 9 times increase in the estimated lifetime. Therefore, it can be concluded that the per-phase MPC method is effective in reducing thermal variation and increasing the lifetime of VSI.

TABLE 4. Calculated junction temperature and estimated lifetime.

	$T_{j,\text{high}}$	$T_{j,\text{low}}$	T_{jm}	ΔT_j	Est. Lifetime
Conventional MPC	93.5 °C	58.5 °C	76 °C	35 °C	3.1 yrs
Proposed MCP	81.3 °C	56.3 °C	68.8 °C	25 °C	27.7 yrs

From the simulation waveforms, experimental waveforms, and output performance comparison, the proposed per-phase MPC technique can successfully decrease the switching loss of the most aged leg of VSI, whereas the output performance is guaranteed as in the conventional MPC method. It can be realized by the significant reduction of loss and similar THD of the load currents for all the operating areas.

V. CONCLUSION

In conclusion, this paper has presented a new effective approach to significantly reduce switching losses of particular phase leg in VSIs using per-phase MPC with preselection of switching state. The proposed method is based on selecting the most appropriate switching state from preselected switching states, which results in a significant reduction in switching losses compared to conventional MPC methods. Additionally, the proposed method does not require any additional sensors or hardware modifications, which makes it easy to implement in existing systems. The efficiency of the proposed technique has been validated through both simulation and experimental results, which show that it is capable of reducing switching losses in a particular phase leg by up to 90%. Due to its non-disruptive characteristics and ability to integrate seamlessly into current systems, the suggested approach exhibits immense promise in enhancing the energy efficiency and performance of VSIs. As a result, it has the potential to bring advantages to a wide range of industries and applications.

REFERENCES

[1] J. Rocabert, A. Luna, F. Blaabjerg, and P. Rodríguez, "Control of power converters in AC microgrids," *IEEE Trans. Power Electron.*, vol. 27, no. 11, pp. 4734–4749, Nov. 2012.
[2] I. Husain, B. Ozpineci, M. S. Islam, E. Gurpinar, G.-J. Su, W. Yu, S. Chowdhury, L. Xue, D. Rahman, and R. Sahu, "Electric drive technology trends, challenges, and opportunities for future electric vehicles," *Proc. IEEE*, vol. 109, no. 6, pp. 1039–1059, Jun. 2021.
[3] M. Rodríguez, A. Rodríguez, P. F. Miaja, D. G. Lamar, and J. S. Zúniga, "An insight into the switching process of power MOSFETs: An improved analytical losses model," *IEEE Trans. Power Electron.*, vol. 25, no. 6, pp. 1626–1640, Jun. 2010.
[4] S. Yang, D. Xiang, A. Bryant, P. Mawby, L. Ran, and P. Tavner, "Condition monitoring for device reliability in power electronic converters: A review," *IEEE Trans. Power Electron.*, vol. 25, no. 11, pp. 2734–2752, Nov. 2010.
[5] S. Yang, A. Bryant, P. Mawby, D. Xiang, L. Ran, and P. Tavner, "An industry-based survey of reliability in power electronic converters," *IEEE Trans. Ind. Appl.*, vol. 47, no. 3, pp. 1441–1451, May 2011.
[6] V. Smet, F. Forest, J.-J. Huselstein, F. Richardeau, Z. Khatir, S. Lefebvre, and M. Berkani, "Ageing and failure modes of IGBT modules in high-temperature power cycling," *IEEE Trans. Ind. Electron.*, vol. 58, no. 10, pp. 4931–4941, Oct. 2011.
[7] H. Oh, B. Han, P. McCluskey, C. Han, and B. D. Youn, "Physics-of-failure, condition monitoring, and prognostics of insulated gate bipolar transistor modules: A review," *IEEE Trans. Power Electron.*, vol. 30, no. 5, pp. 2413–2426, May 2015.
[8] C. M. D. O. Stein, H. A. Grundling, H. Pinheiro, J. R. Pinheiro, and H. L. Hey, "Zero-current and zero-voltage soft-transition commutation cell for PWM inverters," *IEEE Trans. Power Electron.*, vol. 19, no. 2, pp. 396–403, Mar. 2004.
[9] J. Shukla and B. G. Fernandes, "Three-phase soft-switched PWM inverter for motor drive application," *IET Electr. Power Appl.*, vol. 1, no. 1, p. 93, 2007.
[10] P. Sun, J.-S. Lai, H. Qian, W. Yu, C. Smith, and J. Bates, "High efficiency three-phase soft-switching inverter for electric vehicle drives," in *Proc. IEEE Vehicle Power Propuls. Conf.*, Sep. 2009, pp. 761–766.
[11] R. Chen and F. Z. Peng, "A high-performance resonant gate-drive circuit for MOSFETs and IGBTs," *IEEE Trans. Power Electron.*, vol. 29, no. 8, pp. 4366–4373, Aug. 2014.
[12] Z. Wang, X. Shi, L. M. Tolbert, F. Wang, and B. J. Blalock, "A di/dt feedback-based active gate driver for smart switching and fast overcurrent protection of IGBT modules," *IEEE Trans. Power Electron.*, vol. 29, no. 7, pp. 3720–3732, Jul. 2014.
[13] X. Mao, R. Ayyanar, and H. K. Krishnamurthy, "Optimal variable switching frequency scheme for reducing switching loss in single-phase inverters based on time-domain ripple analysis," *IEEE Trans. Power Electron.*, vol. 24, no. 4, pp. 991–1001, Apr. 2009.
[14] L. Wei, J. McGuire, and R. A. Lukaszewski, "Analysis of PWM frequency control to improve the lifetime of PWM inverter," *IEEE Trans. Ind. Appl.*, vol. 47, no. 2, pp. 922–929, Mar. 2011.
[15] Y. Ko, M. Andresen, G. Buticchi, and M. Liserre, "Thermally compensated discontinuous modulation strategy for cascaded H-bridge converters," *IEEE Trans. Power Electron.*, vol. 33, no. 3, pp. 2704–2713, Mar. 2018.
[16] D. A. Murdock, J. E. Ramos, J. J. Connors, and R. D. Lorenz, "Active thermal control of power electronics modules," in *Proc. 38th IAS Annu. Meeting Conf. Rec. Ind. Appl. Conf.*, Salt Lake City, UT, USA, 2003, pp. 1511–1515.
[17] J. Rodriguez, M. P. Kazmierkowski, J. R. Espinoza, P. Zanchetta, H. Abu-Rub, H. A. Young, and C. A. Rojas, "State of the art of finite control set model predictive control in power electronics," *IEEE Trans. Ind. Informat.*, vol. 9, no. 2, pp. 1003–1016, May 2013.
[18] S. Vazquez, J. Rodriguez, M. Rivera, L. G. Franquelo, and M. Norambuena, "Model predictive control for power converters and drives: Advances and trends," *IEEE Trans. Ind. Electron.*, vol. 64, no. 2, pp. 935–947, Feb. 2017.
[19] A. Janabi and B. Wang, "Variable mode model predictive control for minimizing the thermal stress in electric drives," in *Proc. IEEE Int. Electr. Mach. Drives Conf. (IEMDC)*, Miami, FL, USA, May 2017, pp. 1–5.
[20] S. Kwak and J.-C. Park, "Switching strategy based on model predictive control of VSI to obtain high efficiency and balanced loss distribution," *IEEE Trans. Power Electron.*, vol. 29, no. 9, pp. 4551–4567, Sep. 2014.
[21] J. Rodríguez and P. C. Estay, *Predictive Control of Power Converters and Electrical Drives*. Hoboken, NJ, USA: Wiley, 2012.
[22] J.-C. Kim and S. Kwak, "Per-phase switching frequency control method to extend lifespan of three-phase voltage source inverters," *IEEE Access*, vol. 10, pp. 115849–115868, 2022.
[23] J. Kim, M.-H. Nguyen, S. Kwak, and S. Choi, "Lifetime extension method for three-phase voltage source converters using discontinuous PWM scheme with hybrid offset voltage," *Machines*, vol. 11, no. 6, p. 612, Jun. 2023.
[24] L. Asiminoaei, P. Rodriguez, F. Blaabjerg, and M. Malinowski, "Reduction of switching losses in active power filters with a new generalized discontinuous-PWM strategy," *IEEE Trans. Ind. Electron.*, vol. 55, no. 1, pp. 467–471, Jan. 2008.
[25] K. Ma, "Electro-thermal model of power semiconductors dedicated for both case and junction temperature estimation," in *Power Electronics for the Next Generation Wind Turbine System*, vol. 5. Cham, Switzerland: Springer, 2015, pp. 139–143.
[26] *SKM75GB07E3*, Datasheet, SEMIKRON, Nuremberg, Germany, 2021.
[27] S. S. Manson, *Thermal Stress and Low Cycle Fatigue*. New York, NY, USA: McGraw-Hill, 1966.
[28] N. Kaminsku, "Load-cycling capability of HiPak," ABB, Appl. Note 5SYA 2043-01, 2004.
[29] K. Ma, M. Liserre, F. Blaabjerg, and T. Kerekes, "Thermal loading and lifetime estimation for power device considering mission profiles in wind power converter," *IEEE Trans. Power Electron.*, vol. 30, no. 2, pp. 590–602, Feb. 2015.

MINH HOANG NGUYEN received the B.S. degree in electrical and electronics engineering from the Hanoi University of Science and Technology, Vietnam, in 2016. He is currently pursuing the joint M.S. and Ph.D. degree in electrical and electronics engineering with Chung-Ang University, Seoul, South Korea. His research interest includes control for multilevel converters.

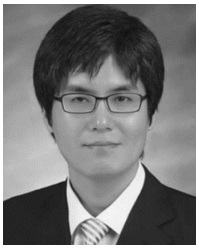

SANGSHIN KWAK (Member, IEEE) received the Ph.D. degree in electrical engineering from Texas A&M University, College Station, TX, USA, in 2005. From 2007 to 2010, he was an Assistant Professor with Daegu University, Gyeongsan, South Korea. Since 2010, he has been with Chung-Ang University, Seoul, South Korea, where he is currently a Professor. His current research interests include the design, modeling, control, and analysis of power converters for electric vehicles and renewable energy systems as well as the prognosis and fault-tolerant control of power electronics systems.

SEUNGDEOG CHOI (Senior Member, IEEE) received the B.S. degree in electrical and computer engineering from Chung-Ang University, Seoul, South Korea, in 2004, the M.S. degree in electrical and computer engineering from Seoul National University, Seoul, in 2006, and the Ph.D. degree in electric power and power electronics from Texas A&M University, College Station, TX, USA, in 2010. From 2006 to 2007, he was a Research Engineer with LG Electronics, Seoul. From 2009 to 2012, he was a Research Engineer with Toshiba International Corporation, Houston, TX, USA. From 2012 to 2018, he was an Assistant Professor with The University of Akron, Akron, OH, USA. Since 2018, he has been an Associate Professor with Mississippi State University, Starkville, MS, USA. His current research interests include degradation modeling, fault-tolerant control, and fault-tolerant design of electric machines, power electronics, batteries, solar panels, and wider vehicular/aircraft microgrid systems.